Eigenchannel R-matrix study of the J=0 and J=2 even parity spectra of calcium below the Ca^+ $3d_{3/2}$ threshold

J. Phys. B: At. Mol. Opt. Phys. 24 (1991) 4935–4956. Printed in the UK

Eigenchannel R-matrix study of the $J = 0$ and $J = 2$ even parity spectra of calcium below the Ca^+ $3d_{3/2}$ threshold

Mireille Aymar and Mourad Telmini
Laboratoire Aimé Cotton, CNRS II, Bâtiment 505, 91405 Orsay Cedex, France

Received 28 May 1991

Abstract. The $J = 0$ and $J = 2$ even parity spectra of calcium are studied through a combination of the eigenchannel R-matrix and multichannel quantum defect (MQDT) methods. The bound and autoionizing spectra below the $3d_{3/2}$ threshold are investigated. The calculation reproduces well the perturbations of the $4snS$ $^1S_0$, $4snd$ $^{1,3}D_2$ series by low-lying doubly excited states observed experimentaly and provides new insight on the identification of the perturbers. Theoretical predictions of the positions of the $3dnl$ and low-lying $4pnp$ $J = 0^e$ and $J = 2^e$ resonances are given. Several photoionization spectra from low-lying states are presented. Particular attention is paid to analyse the effects of the strong interaction between the $3dnd$ and $4pnp$ singlet channels which dominates the bound and autoionizing spectra above the first limit. Comparisons are made with the results of previous experimental and theoretical studies.

1. Introduction

Recently, several theoretical investigations devoted to Ca (Greene and Kim 1987, Kim and Greene 1987, 1988), Sr (Aymar *et al* 1987, Aymar 1987, Kompitsas *et al* 1991, 1992), Ba (Aymar 1990) and Sr to Ra (Greene and Aymar 1991) have shown that a very realistic description of these atoms can be obtained by combining the eigenchannel R-matrix method (Greene 1985, 1988) with the multichannel quantum defect theory (MQDT) (Seaton 1983, Fano and Rau 1986). Theoretical results were found to describe accurately various perturbed Rydberg series and photoionization spectra of ground or excited states. Thus the method is expected to provide valuable new information for spectra where unsolved theoretical problems remain and reliable predicted energies when experimental data are lacking.

This paper deals with the $J = 0$ and $J = 2$ even parity spectra of calcium below the $3d_{3/2}$ limit whereas previous experimental and theoretical investigations have mainly concerned the bound spectra below the 4s limit. Information on the autoionizing energy range is very scarce. Several previous theoretical investigations have been devoted to the analysis of the perturbations of the $4snl$ Rydberg series by low-lying doubly excited states. These calculations are applications of the empirical MQDT method (Armstrong *et al* 1977, Wynne and Armstrong 1979), of variational methods (Nesbet and Jones 1977, Bathia *et al* 1990, Froese Fischer and Hansen 1981, 1985, Vaeck *et al* 1991) or configuration interaction approaches (Friedrich and Trefftz 1969, Nomura and Tatewaki 1982). Disagreements exist between the various authors for the assignments of several perturbers. The main question is which of the two configurations $4p^2$ or $3d^2$ represents the lowest $^1S_0$ and $^1D_2$ perturbers better. For both

0953-4075/91/234935+22$03.50

$^1S_0$ and $^1D_2$ series the lowest perturbers are traditionally labelled $4p^2$; these levels will be referred to in this work as P_0 ($E = 41\,876$ cm^{-1}) and P_2 (40 720 cm^{-1}). The two other singlet doubly excited states commonly labelled as $3d^2\ ^1S_0$ and $^1D_2$ have not been observed, although the $3d^2\ ^1D_2$ seems to affect high-lying $4snd\ ^1D_2$ levels. Where are these levels (referred to as P_0' and P_2' hereafter)?

It is worth noting that the location and assignment of the singlet levels of d^2 and p^2 configurations of strontium and barium have often been questioned. Since the recent observation of the $5p^2\ ^1S_0$ of strontium by Kompitsas *et al* (1991), in contrast with calcium, all the singlet levels of d^2 and p^2 configurations are known. Several calculations done with the eigenchannel R-matrix method have aimed to analyse the influence of the dd–pp interaction on the positions and wavefunctions of these singlet levels (Aymar *et al* 1987, Kompitsas *et al* 1991, 1992, Greene and Aymar 1991). In particular these studies have confirmed that the $5p^2\ ^1S_0$ level of Sr and $6p^2\ ^1S_0$ level of Ba correspond to broad autoionizing resonances, while initialy the $p^2\ ^1S_0$ label was given to bound levels. A major purpose of the present study is to extend the analysis of the dd–pp interaction to calcium and to get predictions for the unobserved levels P_0' and P_2'.

With regard to the autoionizing energy range, recent measurements and theoretical analyses concern high-lying doubly excited states above the 4p threshold (Morita and Suzuki 1990 and reference therein). But the lower energy range has been less thoroughly studied, available data concerning only a few levels (Sugar and Corliss 1985). Thus predicted energy positions for doubly excited states pertaining to $3dnl$ series are of particular interest.

This paper presents new theoretical results on the perturbed Rydberg series $4sns\ ^1S_0$ and $4snd\ ^{1,3}D_2$, on the position of $J = 0^e$ and $J = 2^e$ doubly excited states and on various photoionization spectra involving these states as final states. The eigenchannel R-matrix method is used to calculate variationally the short-range parameters used by MQDT to describe channel interactions. R-matrix calculations are performed in LS coupling and the geometric frame transformation (jj/LS) is employed to account for fine structure effects. All previous theoretical studies devoted to the $J = 0$ and $J = 2$ even parity spectra of calcium were conducted in pure LS coupling and it is worthwhile to analyse the role of the spin–orbit interaction. All the experimental energy values used in this work for the Ca and Ca^+ spectra are extracted from the recent compilation done by Sugar and Corliss (1985), hereafter to be referred to as SC.

2. Theory

The computational procedure which combines the eigenchannel R-matrix approach with MQDT has been presented in detail in various papers (Greene 1985, Greene and Kim 1987, Aymar *et al* 1987, Aymar 1987, 1990, Greene and Aymar 1991) and only some key points are outlined here.

Eigenchannel R-matrix calculations are performed in LS coupling. The wavefunctions of the pair of electrons outside a frozen core are calculated within a finite volume V, using a variational expression for the normal logarithmic derivative on the surface S of V. A reaction volume of radius $r_0 = 15$ au is used. The two-electron basis functions are antisymmetrized products of one-electron orbitals coupled to form a state of given S, L and parity. The one electron orbitals are numerical solutions of the Ca^{2+}–e Schrödinger equation where a model potential is used to describe the

Table 1. Empirical parameters involved in the model potential.

	l	α_1	α_2	α_3	r_c
	0	4.0099	13.023	2.1315	1.6352
$\alpha_d = 3.5$	1	4.2056	12.658	2.0186	1.5177
	2	3.5058	12.399	2.2648	1.6187
	$\geqslant 3$	3.7741	13.232	3.1848	0.7150

Ca^{2+}–e interaction. Because the 3d orbital of Ca is known to be extremely sensitive to screening, we use a more elaborate model potential than in previous calculations done in calcium (Greene and Kim 1987, Kim and Greene 1987). As in recent calculations done in Sr, Ba and Ra (Aymar 1990, Kompitsas *et al* 1991, 1992, Greene and Aymar 1991), the potential $U(r)$ includes a screening term and a polarization term, both terms being l-dependent:

$$U(r) = -\frac{1}{r}[2 + 18\exp(-\alpha_1^l r) + \alpha_2^l r \exp(-\alpha_3^l r)] - \frac{\alpha_d}{2r^4}\left\{1 - \exp\left[-\left(\frac{r}{r_c^l}\right)^6\right]\right\}$$

where α_d is the dipole polarizability of the Ca^{2+} ion. The empirical parameters α_i and r_c^l are adjusted until the energy levels of the one-electron Schrödinger equation reproduce accurately the average spin–orbit energies of Ca^+ experimental levels. The values of the parameters are given in table 1.

Independent eigenchannel R-matrix calculations are done for $^1S^e$, $^3P^e$, $^1D^e$, $^3D^e$ and $^3F^e$ symmetries involved in even parity $J = 0$ and $J = 2$ spectrum of Ca below the $3d_{3/2}$ limit. The channels involved in these calculations are displayed in table 2. These channels correspond to open or 'weakly closed' channels in which the outermost electron can escape from the reaction volume. Additional 'strongly closed' channels are accounted for in the variational calculations. These latter channels which contribute at short range but are exponentially small on the surface S of the reaction volume account for various polarization and correlation effects.

Table 2. LS-coupled and jj-coupled dissociation channels introduced respectively in the R-matrix and MQDT calculations.

LS-coupled channels

^1S	4s*n*s	3d*n*d	4p*n*p	
^3P	3d*n*d	4p*n*p		
^1D	4s*n*d	3d*n*s	3d*n*d	4p*n*p
^3D	4s*n*d	3d*n*s	3d*n*d	4p*n*p
^3F	3d*n*d			

jj-coupled channels

Threshold	$J = 0$	$J = 2$
$4s_{1/2}$	$4s_{1/2}ns_{1/2}$	$4s_{1/2}nd_{3/2}$, $4s_{1/2}nd_{5/2}$
$3d_{3/2}$	$3d_{3/2}nd_{3/2}$	$3d_{3/2}ns_{1/2}$, $3d_{3/2}nd_{3/2}$, $3d_{3/2}nd_{5/2}$
$3d_{5/2}$	$3d_{5/2}nd_{5/2}$	$3d_{5/2}ns_{1/2}$, $3d_{5/2}nd_{3/2}$, $3d_{5/2}nd_{5/2}$
$4p_{1/2}$	$4p_{1/2}np_{1/2}$	$4p_{1/2}np_{3/2}$
$4p_{3/2}$	$4p_{3/2}np_{3/2}$	$4p_{3/2}np_{1/2}$, $4p_{3/2}np_{3/2}$

The R-matrix calculation gives the logarithmic derivatives of the escaping electron's wavefunctions on the surface S which are converted into smooth LS-coupled short-range reaction matrices K^{LS}. These matrices are determined as explicit functions of the energy E, by performing R-matrix calculations on a selected grid of E. Using the (jj/LS) geometric frame transformation the K^{LS} matrices are recoupled into larger jj-coupled reaction matrices K^J referring to jj-coupled dissociations channels. The channels connected by the $K^{J=0}$ and $K^{J=2}$ matrices are displayed in table 2. Let us note that for the $J = 2^e$ spectrum, the 3dng channels, assumed to be only very weakly coupled to the 3dnd and 3dns channels, are not introduced explicitly in the calculations, but accounted for implicitly by treating them as 'strongly closed' in the R-matrix calculations.

The energy-dependent reaction matrices $K^{J=0}$ and $K^{J=2}$ furnish all the information to characterize channel mixing in the $J = 0^e$ and $J = 2^e$ spectra. Calculation of photoionization cross sections requires, in addition, the calculation of dipole matrix elements connecting the initial state to the R-matrix eigenstates. Photoionization processes considered in this work involve low-lying states as initial states. These states are assumed to be contained within the reaction volume V and their wavefunctions are obtained by diagonalizing the two-electron Hamiltonian within V using a finite two-electron basis.

The calculation of observable quantities from the energy-dependent MQDT parameters proceeds by standard MQDT techniques (Lu 1971, Lee and Lu 1973). The MQDT parameters are the eigenvalues μ_α, the eigenvectors $U_{i\alpha}$ of the K matrix and the D_α dipole matrix elements. The index α refers to the short-range eigenchannels and i refers to the jj-coupled dissociation channels.

In the autoionizing range, MQDT techniques adapted to bound spectra can be used to obtain resonance positions providing that the complete K matrix connecting open and closed channels is replaced by an effective reaction matrix. As detailed by Fano and Rau (1986), Lecomte (1987), Kompitsas *et al* (1990) and Aymar (1990), this effective reaction matrix K_{eff} corresponds to the real part of the contracted matrix κ_{cc} restricted to the closed channels

$$\kappa_{cc} = K_{cc} - K_{co}(iI_{oo} + K_{oo})^{-1}K_{oc}$$

where c denotes the closed channels, o the open channels and I a unit matrix.

Calculation of admixture coefficients Z_i of dissociation channels i into each level enables us to quantitatively analyse channel mixing and to identify the levels. Graphic representation of channel mixing is obtained by using Lu–Fano plots which, in the discrete spectrum, consist of a plot of $-\nu_i$ (mod 1) against ν_j for chosen pairs of effective quantum numbers ν_i and ν_j; the extension of the Lu–Fano graph above the ith threshold consists of a graph of the phaseshifts τ against ν_j.

It must be finally noted that fine-structure effects are accounted for in the MQDT calculations where experimental energies (including fine-structure splitting) are used for the ionization thresholds. As explained by Aymar (1990) and Greene and Aymar (1991), this procedure sometimes leads to inaccuracies at the low energy end of closed channels because there the MQDT parameters acquire a strong energy dependence and thus results become very sensitive to the threshold energy. These difficulties which arise here at the low energy end of the 4pnp channel are removed by using theoretical energies instead of experimental ones for the 4p threshold energy in the MQDT calculations devoted to the bound spectra.

3. Even parity $J = 0$ spectrum

3.1. Bound spectrum

Below the first limit, the $J = 0^e$ spectrum consists of the $4sns\ ^1S_0$ series and three doubly excited states. Although the $4sns\ ^1S_0$ series seems to be perturbed only by the singlet doubly excited state P_0 (see introduction) and not by the $4p^2\ ^3P_0$ and $3d^2\ ^3P_0$ states, a five channel MQDT analysis is performed. The relevant channels are given in table 2. The Lu–Fano plot displayed in figure 1 shows that the R-matrix calculation perfectly describes the perturbation of the $4sns\ ^1S_0$ series by the P_0 perturber. The agreement between theory and experiment is comparable to that obtained by Armstrong *et al* (1977) who used a two-channel MQDT model fitted to experiment (see their figure 5). More detailed comparison between calculated and fitted MQDT parameters will be given in section 5. In addition, the five-channel MQDT calculation permits good reproduction of the energy positions of the triplet levels $4p^2\ ^3P_0$ and $3d^2\ ^3P_0$ (as visible from table 3). It clearly appears that these levels do not perturb the $4sns\ ^1S_0$ series justifying the assumption of negligible spin–orbit effects by Armstrong *et al* (1977). The right part of figure 1 where each rise of the phase shift corresponds to an autoionizing resonance will be commented on in section 3.2.

Table 3. Comparison of the energy positions (in cm^{-1}) of low-lying doubly excited states calculated in this work with previous experimental data (SC).

Label (SC)	E_{exp}	E_{the}	ΔE
$J = 0$			
$4p^2\ ^3P$	38417	38400	17
P_0	41786	41854	−68
$3d^2\ ^3P$	49524	49846	−322
$3d4d\ ^3P$	54282	54461	−179
$3d5d\ ^3P$	57611	57675	−64
$J = 2$			
$4p^2\ ^3P$	38552	38428	124
P_2	40720	40767	−47
$3d^2\ ^3F$	43475	43770	−225
$3d5s\ ^1D$	47449	47451	−2
$3d5s\ ^3D$	47466	47485	−19
$3d^2\ ^3P$	48564	48856	−292
$3d4d\ ^3D$	51369	51381	−12
$3d4d\ ^3F$	53215[a]	53966	−741
$3d4d\ ^3P$	54305	54501	−196
$3d5d\ ^3D$	56469	56476	−7
$3d5d\ ^3P$	57638	57706	−68
$3d6d\ ^3P$[b]	59391	59381	10

[a] The existence of the level at 53215 cm^{-1} was questioned by Risberg (1968).
[b] This level is labelled $3d_{5/2}6d_{3/2}$ in table 7.

Now we turn to the composition of the wavefunction of the P_0 level. Results obtained in this work for the energy and the pp and dd percentage characters of the P_0, P_0', P_2 and P_2' doubly excited states are compared in table 4 with previous theoretical values. Results (a) are obtained with the R-matrix method which gives

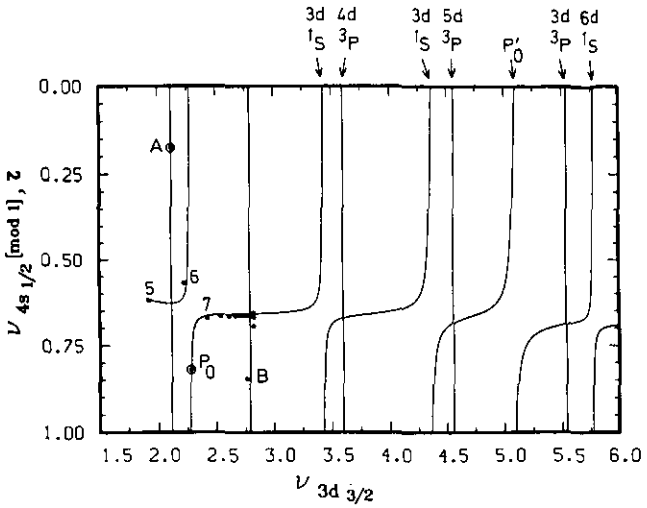

Figure 1. Lu–Fano plot of the $J = 0^e$ spectrum. The solid line $-\nu_{4s_{1/2}}$ (mod 1)$=f(\nu_{3d_{3/2}})$ or $\tau = f(\nu_{3d_{3/2}})$ is calculated with the *jj*-coupled reaction matrix $K^{J=0}$; the symbols for experimental level positions (SC) are: (●) 4s*n*s labelled by their *n* value, (⊙) doubly excited states: P_0, A: $4p^2\ ^3P_0$, B: $3d^2\ ^3P_0$. Above the 4s threshold ($\nu_{d_{3/2}} = 2.835$), vertical arrows at the top indicate the positions of the autoionizing resonanaces.

quantitative information on the wavefunctions of low-lying levels contained within the reaction volume. Results (b) and (c) correspond to the MQDT calculations. Previous values (d) to (h) were obtained with the MCHF method (Froese Fischer and Hansen 1981, 1985, Vaeck *et al* 1991), the Bethe and Goldstone approach (Nesbet and Jones 1977) or by configuration mixing methods (Friedrich and Trefftz 1969, Nomura and Tatewaki 1982). Only results obtained by accounting for the d^2–p^2 interaction are quoted in table 3. For the P_0 level, the present calculations confirm previous results, i.e. the pp and dd components have the same order of magnitude. At this point it is not possible to give a label to the P_0 perturber and this problem will be discussed further in the following sections.

3.2. Energy positions of the autoionizing resonances

A preliminary analysis of the positions of autoionizing resonances has been performed in *LS* coupling. The positions of ^{3}P resonances are obtained from the $K^{^3P}$ reaction matrix while the positions of ^{1}S resonances are obtained with the effective reaction matrix $K^{^1S}_{eff}$ restriction of $K^{^1S}$ to the closed channels 3d*n*d and 4p*n*p ^{1}S. The two independent Lu–Fano plots of the ^{1}S and ^{3}P states on the ν_{3d} (mod 1) against ν_{4p} are displayed in figure 2(*a*) (figure 2(*b*) will be commented on in section 4). The effective quantum numbers ν_{3d} and ν_{4p} correspond to the 3d and 4p theoretical ionization limits very close to the experimental average spin–orbit split ionization limits. The points indicate theoretical energy positions of autoionizing levels located between the 4s and 3d ionization limits. For the ^{1}S curve the sharp increase of ν_{3d} near $\nu_{4p} = 2.64$ clearly indicates the 3d*n*d ^{1}S series is perturbed there by a 4p*n*p ^{1}S state. All the states located between the 4s and 3d thresholds have no more than 6% pp character except those at 58700 and 59650 cm^{-1} with respectively 25% and 18% pp character. This suggests the level at 58700 cm^{-1} is the P'_0 level

Table 4. Energy positions and pp and dd percentage character of singlet levels of $4p^2$ and $3d^2$ configurations. The MQDT characters (b, c)correspond to W_i coefficients defined by the relation $W_i = Z_i^2 / \sum_k (Z_k)^2$. The characters (a) and (d) to (g) are obtained by adding all squared contributions of the same type in a given eigenvector.

Experiment (SC)				Theory		% character	
E (cm^{-1})	Label	Present label		E (cm^{-1})	ΔE (cm^{-1})	pp	dd
			a	42030	−244	39	54
			b	41844	−58	39	54
			d	40939	847	47	39
41786	$4p^2\ ^1S_0$	P_0	e	40980	806	46	41
		'$3d^2$' $^1S_0$	f	41077	709		
			g	43168	−1382	29	57
			h	41740	46	51	32
		P_0'	b	58715			
	$3d^2\ ^1S_0$	'$4p^2$' $^1S_0$	c	58705		30	70
			f	59069			
			a	41583	−863	30	41
			b	40767	−47	18	66
40720	$4p^2\ ^1D_2$	P_2	e	40246	474	40	21
		'$3d^2$' $^1D_2$	f	42675	−1955		
			g	41509	−789	20	27
		P_2'	b	49526			
	$3d^2\ ^1D_2$	'$4p^2$' $^1D_2$	c	49698		47	44
			f	59069			

Results a to c are obtained in the present work:

[a] From the wavefunctions composition within a finite reaction volume of radius $r_0 = 18$ au.

[b] MQDT calculation with K^J; above the 4s threshold, the energy position correspond to the cross-section maximum.

[c] MQDT calculation with K_{eff}^J; results obtained with K_{eff}^{LS} are almost the same.

[d] MCHF calculation (Froese Fischer and Hansen 1981, 1985).

[e] MCHF calculation (Vaeck *et al* 1991).

[f] Bethe and Goldstone approach (Nesbet and Jones 1977). The lowest $^1S_0$ level is said to have equal weight from $4p^2$ and $3d^2$ configurations and the lowest $^1D_2$ to have nearly equal weight from the three configurations 4s3d, $4p^2$ and $3d^2$.

[g] CI calculation. Friedrich and Treffitz (1969).

[h] CI calculation. Nomura and Tatewaki (1982).

strongly interacting with the P_0 bound level (see table 4). Since lower levels are identified as members of the 3d*n*d ^1S series, this level has to be identified as the '$4p^2$' $^1S_0$ level. This leads us to reverse the label previously given in the literature, identifying P_0 as the '$3d^2$' $^1S_0$ level even if several calculations predict its 4p*n*p character to be larger than the dd character. A better conclusion is that single particle labels are not adequate for such strongly correlated levels. Now consider the ^3P branch of figure 2(*a*). The rapid increase of ν_{3d} just below the 3d threshold gives evidence that the 3d*n*d ^3P series is perturbed by a 4p*n*p ^3P state. The state involved is the 4p5p ^3P state which is diluted into the high-lying members of the 3d*n*d ^3P series and probably also affects the autoionizing spectrum above the 3d threshold.

This treatment in *LS* coupling has been completed by a four-channel analysis based on the *jj*-coupled reaction matrix $K_{\text{eff}}^{J=0}$ referring to the four 3d*n*d and 4p*n*p

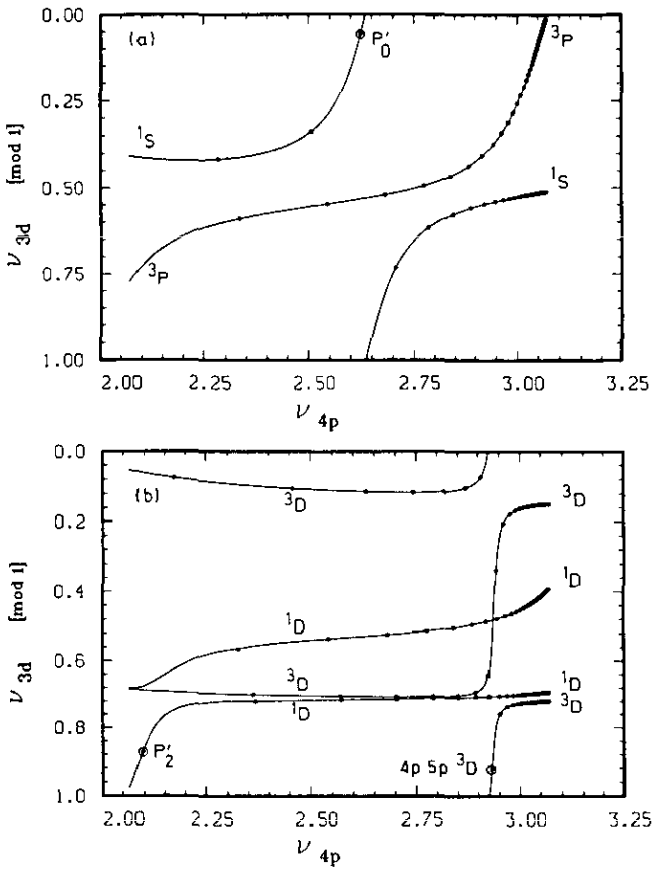

Figure 2. Lu–Fano plot of autoionizing levels in the $-\nu_{3d}$ (mod 1) against ν_{4p} plane. The curves and theoretical energies are calculated with *LS*-coupled reaction matrices: (*a*) ^{1}S and ^{3}P series; (*b*) ^{1}D and ^{3}D series.

closed channels. The theoretical Lu–Fano plot of the $J = 0^e$ levels on the $-\nu_{3d_{3/2}}$ (mod 1) against $\nu_{3d_{5/2}}$ is displayed in figure 3. The squares correspond to experimental levels (SC) and the dots to predicted $J = 0^e$ levels expected to lie between the 4s and $3d_{3/2}$ thresholds. The shape of the curve considerably differs from a two-channel Lu–Fano plot describing two weakly coupled Rydberg series converging to two different fine structure levels. The absence of a horizontal branch indicates that the $3d_{3/2}nd_{3/2}$ $J = 0$ series is strongly coupled to the $3d_{5/2}nd_{5/2}$ series. The behaviour of 3d*n*d $J = 0$ series of Ca differs from that of 4d*n*d $J = 0$ series of Sr and 5d*n*d $J = 0$ series of Ba. This can be seen by comparing figure 3 with figure 8 of Kompitsas *et al* (1991) obtained in Sr and the figure 6 of Aymar *et al* (1983) dealing with Ba. The differences in channel structure patterns are related to the differences in the perturbations of the $(m_0 - 1)$d*n*d series by low members of the m_0p*n*p series ($m_0 = 4$, 5 and 6 for Ca, Sr and Ba respectively). The 5d*n*d $J = 0$ series of Ba are perturbed by the $6p^2\ ^1S_0$ level while the 4d*n*d $J = 0$ series of Sr interacts with the $5p^2\ ^1S_0$ and $5p6p\ ^3P_0$ levels. However these levels affect the low members of the $(m_0 - 1)$d*n*d series only and in a large spectral range below the $(m_0 - 1)d_{3/2}$ threshold the Lu–Fano plots display a two-channel regular pattern corresponding to a

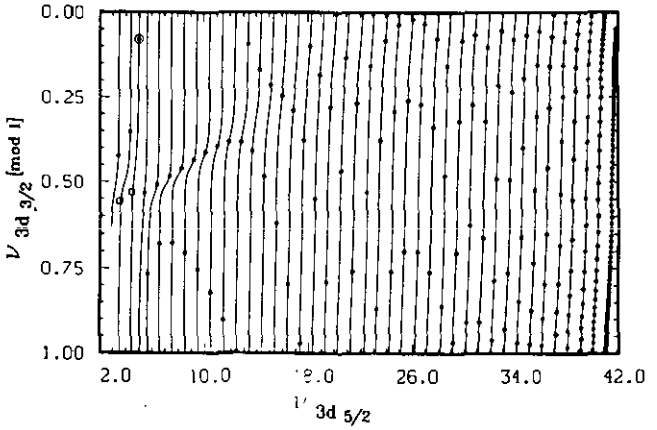

Figure 3. Lu–Fano plot of the autoionizing $J = 0^e$ levels in the $-\nu_{3d_{3/2}}$ (mod 1) against $\nu_{3d_{5/2}}$ plane, below the $3d_{3/2}$ threshold ($\nu_{d_{5/2}} = 42.522$). The curves and theoretical energy levels (●) are calculated with *jj*-coupled effective reaction matrix $K_{\text{eff}}^{J=0}$. (⊙): corresponds to the P_0' level and the squares to experimental levels (sc).

$(m_0-1)d_{3/2}nd_{3/2}$ series weakly perturbed periodically by the $(m_0-1)d_{5/2}nd_{5/2}$ levels. The complicated pattern displayed in figure 3 is due to the perturbation of the 3d*n*d $J = 0$ series by the '$4p^2$' $^1S_0$ (P_0' perturber) and 4p5p $^3P_0$ levels, the dd–pp coupling inducing a mixing between the $(m_0 - 1)nd$ $J = 0$ series of Ca larger than in Sr and Ba.

Table 5. MQDT parameters calculated with the *R*-matrix method for the $J = 0^e$ spectrum of Ca, Sr and Ba at the $(m_0-1)d_{3/2}$ threshold. The μ_α and $U_{i\alpha}$ parameters correspond to the $(m_0 - 1)dnd\ ^3P_0$ and $^1S_0$ eigenchannels.

		Ca ($m_0 = 4$)		Sr ($m_0 = 5$)		Ba ($m_0 = 6$)	
α		1	2	1	2	1	2
μ_α		0.41	0.62	0.478	0.488	0.51	0.39
	i=1	0.69	0.48	0.71	0.59	0.77	0.63
	i=2	−0.57	0.59	−0.58	0.73	−0.63	0.77
$U_{i\alpha}$	i=3	0.36	−0.37	0.32	−0.20	0.08	0.01
	i=4	−0.25	−0.53	−0.23	−0.28	−0.05	0.01
$\mu_1 - \mu_2$		−0.21		−0.01		0.12	

$\alpha = 1$ $(m_0 - 1)dnd\ ^3P_0$
$\alpha = 2$ $(m_0 - 1)dnd\ ^1S_0$

$i = 1$ $(m_0 - 1)d_{3/2}nd_{3/2}$
$i = 2$ $(m_0 - 1)d_{5/2}nd_{5/2}$
$i = 3$ $m_0p_{1/2}np_{1/2}$
$i = 4$ $m_0p_{3/2}np_{3/2}$

More quantitative comparison of the channel mixing in Ca, Sr and Ba can be obtained from the MQDT parameters deduced from the four-channel $K_{\text{eff}}^{J=0}$ reaction matrices calculated with the *R*-matrix method. Values obtained near the $(m_0 - 1)d_{3/2}$ threshold for the μ_α and $U_{i\alpha}$ parameters associated with $(m_0 - 1)dnd\ ^3P_0$ and $^1S_0$ eigenchannels are displayed in table 5. Values for Sr and Ba correspond to unpublished intermediate results obtained by Kompitsas *et al* (1991) and Greene and Aymar (1991) respectively. The 5d*n*d eigenchannels of Ba are almost uncoupled with

the 6pnp channels while strong mixing occurs between the 3dnd and 4pnp channels of Ca (and between 4dnd and 4pnp channels of Sr)—compare the $U_{3\alpha}$ and the $U_{4\alpha}$ matrix elements. Although the U_{21} and U_{12} matrix elements have comparable magnitude in Ca and Sr, strong differences occur for the $(m_0 - 1)$dnd series of Ca and Sr. In fact the strength of the coupling between the two $J = 0$ series depends not only on the $U_{i\alpha}$ matrix elements but also on the $\Delta\mu = \mu_1 - \mu_2$ value. This point has been shown analytically by Giusti-Suzor and Fano (1984) for the case of two interacting channels. The differences between Ca and Sr result from the fact that $|\Delta\mu|$ is very large in Ca and particularly small in Sr. For two $(m_0 - 1)n$d series not coupled to other series, $\Delta\mu$ is expected to be positive since for a given n the $^1S_0$ level lies above the $^3P_0$ one. As visible in table 5, such property holds in Ba near the $5d_{3/2}$ threshold but not in Ca and Sr because of the strong dd–pp mixing.

Table 6. Energy positions, effective quantum numbers and LS designations of $J = 0^e$ autoionizing resonances below 62 500 cm^{-1}. The first column corresponds to the positions of maxima in the calculated photoionization spectra 4s5p $^1P_1 \longrightarrow J = 0^e$. The energies in the second column, effective quantum numbers and labels are obtained from $K_{\text{eff}}^{J=0}$.

E_σ (cm^{-1})	$E_{K_{\text{eff}}}$ (cm^{-1})	$\nu_{d_{5/2}}$	$\nu_{d_{3/2}}$	Label	(LS)
53596	53597.9	3.41	3.42	3d4d	$^1S_0$
54461	54462.1	3.58	3.59	3d4d	$^3P_0$
57155	57165.6	4.33	4.35	3d5d	$^1S_0$
57675	57675.5	4.53	4.55	3d5d	$^3P_0$
58715	58705.0	5.04	5.08	'4p^2'	$^1S_0$
59371	59377.8	5.49	5.43	3d6d	$^3P_0$
59657	59659.7	5.72	5.76	3d6d	$^1S_0$
60366	60373.1	6.44	6.51	3d7d	$^3P_0$
60496	60497.1	6.60	6.67	3d7d	$^1S_0$
60996	61004.5	7.38	7.48	3d8d	$^3P_0$
61093	61094.8	7.56	7.67	3d8d	$^1S_0$
61422	61430.3	8.32	8.46	3d9d	$^3P_0$
61508	61508.9	8.53	8.68	3d9d	$^1S_0$
61723	61731.3	9.24	9.43	3d10d	$^3P_0$
61803	61803.6	9.51	9.72	3d10d	$^1S_0$
61944	61951.9	10.15	10.46	3d11d	$^3P_0$
62019	*62019.8*	*10.49*	*10.77*	*3d11d*	$^1S_0$
62111	62118.7	10.53	11.39	3d12d	$^3P_0$
62182	62182.6	11.47	11.84	3d12d	$^1S_0$
62240	62248.1	11.95	12.37	3d13d	$^3P_0$
62306	62308.0	12.44	12.92	3d13d	$^1S_0$
62343	62350.8	12.84	13.36	3d14d	$^3P_0$
62403	62406.1	13.40	14.01	3d14d	$^1S_0$
62427	62434.1	13.72	14.37	3d15d	$^3P_0$
62498	62483.4	14.43	15.09	3d15d	$^1S_0$

The energy positions of predicted $J = 0^e$ levels located below 62500 cm^{-1} are compiled in table 6. These values differ from those computed by neglecting spin–orbit effects, mainly in high-energy range below the $3d_{3/2}$ threshold. The assumption of negligible spin–orbit effects justified below the 4s threshold is no longer valid near the $3d_{3/2}$ threshold. The wavefunction composition of 3dnd levels strongly evolves with n and no pure coupling, either jj or LS, holds for most levels. Below 62500 cm^{-1},

LS labels are given in table 6, such a designation being more suitable than *jj*-label for most levels. Predicted energy and wavefunction composition of the P'_0 level are almost identical to those obtained in *LS* calculation, confirming that the '$4p^{2}$' $^1S_0$ label is most suitable for this level. This level strongly affects the low-lying 3d*n*d $^1S_0$ levels which are repelled below the corresponding $^3P_0$. Above 62500 cm^{-1}, it is quite impossible to give a label to the levels, mainly in the high-energy range where the 4p5p $^3P_0$ level is spread out over various levels.

3.3. *Photoionization spectra*

We have calculated the photoionization spectra corresponding to the 4s4p $^1P_1 \longrightarrow J = 0^e$ and 4s5p $^1P_1 \longrightarrow J = 0^e$ spectra. The position of the resonant peaks do not depend on the initial state while their intensity depends on the starting level. Only results corresponding to the 4s5p $^1P_1$ initial state are presented here, in figure 4 and in table 4. All of the peaks but the lowest ones are very narrow. The widths of the resonant peaks are related to the gaps between the branches of the curve $\tau = f(\nu_{d_{3/2}})$ displayed in figure 1, whose size measures the strength of the interaction of the 3d*n*d and 4p*n*p series with the 4sεs continuum. The narrower resonances correspond to 3d*n*d $^3P_0$ autoionizing levels and the largest one to the P'_0 doubly excited state. It is interesting to note the resonance ascribed to the '$4p^{2}$' $^1S_0$ level (P'_0) with a width $\Gamma \sim 80$ cm^{-1} is narrower than the homologous $5p^2$ $^1S_0$ of Sr ($\Gamma \sim 230$ cm^{-1}) (Kompitsas *et al* 1991) and $6p^2$ $^1S_0$ of Ba ($\Gamma \sim 300$ cm^{-1}) (Aymar *et al* 1982). The two levels 3d4d $^3P_0$ and 3d5d $^3P_0$ previously observed (SC) are depicted by vertical arrows. These levels are very difficult to excite from a $^1P_1$ state and correspond to very weak peaks (depicted by vertical bars) close to the experimental observations. The members of the 3d*n*d $^1S_0$ and 3d*n*d $^3P_0$ series are marked by vertical bars drawn at different ordinates. The height of the peaks varies irregularly along each series, the 3d4d $^3P_0$, 3d5d $^1S_0$ and 3d7d $^1S_0$ and $^3P_0$ levels being particularly difficult to excite from the 4s5p $^1P_1$ level.

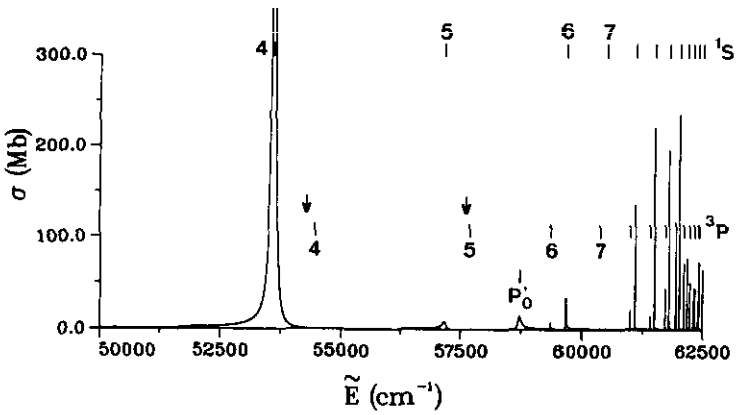

Figure 4. Calculated photoionization cross sections for the 4s5p$^1P_1 \longrightarrow J = 0^e$ process below 62500 cm^{-1}. The vertical bars depict the various members of the two 3d*n*d $^3P_0$ and $^1S_0$ series as well as the P'_0 level. The vertical arrows indicate the positions of the observed resonances (SC).

4. The $J = 2$ even parity spectrum

4.1. Bound spectrum

Below the 4s ionization limit, the $J = 2^e$ spectrum consists of the Rydberg series 4s*n*d $^1D_2$ and $^3D_2$ and of doubly excited states pertaining to the $3d^2$, 3d5s and $4p^2$ configurations. Neglecting spin–orbit effects, Armstrong *et al* (1977) have fitted empirical MQDT models to their experimental data treating separately the triplets and singlets. The perturbation of the 4s*n*d $^3D_2$ series by the 3d5s $^3D_2$ level was reproduced by a two-channel model (4s*n*d+3d*n*s) while a four-channel treatment (4s*n*d+3d*n*s+3d*n*d+4p*n*p) was used to analyse the perturbation of the 4s*n*d $^1D_2$ series by the doubly excited states 3d5s $^1D_2$, P_2 (labelled there as $4p^2$ $^1D_2$) and P_2' ($3d^2$ $^1D_2$). The validity of these empirical models will be discussed further in section 5.

We performed an 11-channel treatment using the $K^{J=2}$ short-range reaction matrix. Figure 5 compares the theoretical Lu–Fano plot with experimental data (SC). The perturbation of the $^1D_2$ series by the low-lying P_2 level is as well described as by Armstrong *et al* (1977) (see their figure 10) while some larger discrepancies are visible in the high-energy range, our calculated energies for the 4s*n*d $^1D_2$ and $^3D_2$ being larger than the experimental ones. However for $n > 30$ the deviations are always smaller than 1 cm^{-1}. Accounting for the large energy dependence of the MQDT parameters, good representation of the low-lying 4s3d $^1D_2$ and $^3D_2$ levels is obtained while, as discussed by Armstrong *et al* (1977), it is difficult to fit these low-lying levels using empirical MQDT models. The avoided crossings between the various branches of the Lu–Fano plot are hardly visible, justifying the treatment done by Armstrong *et al* (1977) which neglects the $^1D_2$–$^3D_2$ mixing as well as the interaction of the 4s*n*d series with the $^3P_2$ and $^3F_2$ doubly excited states. Table 3 shows that the energies of doubly excited states located below the first limit are correctly reproduced by our calculation.

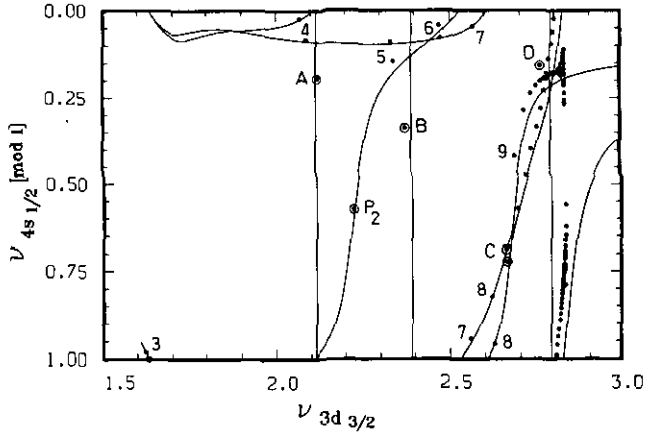

Figure 5. Lu–Fano plot of the $J = 2^e$ bound levels in the $-\nu_{4s_{1/2}}$ (mod 1) against $\nu_{3d_{3/2}}$ plane. The solid line is calculated with the *jj*-coupled reaction matrix $K^{J=2}$; the symbols for experimental level positions (SC) are: (●) 4s*n*d labelled by their *n* value, (⊙) doubly excited states: P_2, A: $4p^2$ $^3P_2$, B: $3d^2$ $^3F_2$, C: 3d5s $^{1,3}D_2$, D: $3d^2$ $^3P_2$.

The *R*-matrix calculation permits the previous assignment of the levels to be checked. Our work confirms the previous labels given to the $4p^2$ $^3P_2$, $3d^2$ $^3F_2$, $3d^2$

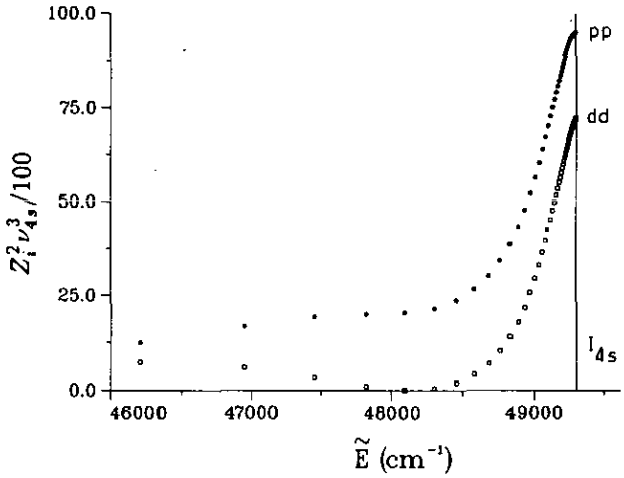

Figure 6. Admixture per unit energy range of 3d*n*d (□) and 4p*n*p (●) $^1D_2$ channels in the bound $^1D_2$ levels. These coefficients are calculated with K^{1D}.

$^3P_2$ and the 3d5s $^{1,3}D_2$ levels. The labelling of the P_2 and P_2' doubly excited states is less evident. Figure 6 displays the admixture per unit energy range ($Z_i^2\nu_{4s}^3$) of 3d*n*d and 4p*n*p $^1D_2$ channels into the high-lying $^1D_2$ levels. The 3d5s $^1D_2$ level and high-lying members of the 4s*n*d $^1D_2$ series have significant admixture of both channels, the admixture of the 4p*n*p channel being the largest. This figure can be compared with figure 9 of Armstrong *et al* (1977) which, however, assumes that the P_2' level is the $3d^2$ $^1D_2$ level and that this level does not interact with the P_2 level identified with the $4p^2$ $^1D_2$ level. Figure 6 confirms that no level corresponds to the P_2' level. Although the P_2' and P_2 levels cannot be ascribed adequately by single particle labels, our calculation (see table 4) indicates that it is better to reverse the labels used in the literature, identifying the P_2 level with the '$3d^2$' $^1D_2$ level and the P_2' level with the '$4p^2$' $^1D_2$ level.

4.2. Energy positions of autoionizing resonances

As in the $J = 0^e$ case, the positions of the 4p*n*p perturbers of the 3d*n*s,*n*d $J = 2$ Rydberg series were deduced from *LS*-coupled reaction matrices. The independent Lu–Fano plots of ^1D and ^3D states in the ν_{3d} (mod 1) against ν_{4p} plane are drawn in figure 2(*b*). Two states having a large pp character are found, corresponding to the sharp rise of the ^1D branch just above the 4s threshold and to the discontinuity of the ^3D branch around $\nu_{4p} = 2.9$. The lower state at $E = 49696$ cm^{-1} with large admixture of both pp and dd channels (see table 4) corresponds to the P_2' level. The higher state at 61871 cm^{-1} is identified with the 4p5p $^3D_2$ state. The 4p5p $^1D_2$ level is found to lie above the 3d threshold. Finally the 3d*nl* $J = 2$ levels are expected to be perturbed by three 4p*n*p $J = 2$ levels: P_2', 4p5p $^3D_2$ and 4p5p $^3P_2$. (See section 3.2 and figure 2.)

This treatment in *LS* coupling has been completed by a nine-channel analysis based on the *jj*-coupled effective reaction matrix referring to 3d*nl* and 4p*n*p closed channels. The theoretical Lu–Fano plot of the $J = 2^e$ levels in the $-\nu_{d_{3/2}}$ (mod 1) against $\nu_{d_{5/2}}$ plane is displayed in figure 7(*a*) and (*b*). The squares correspond to

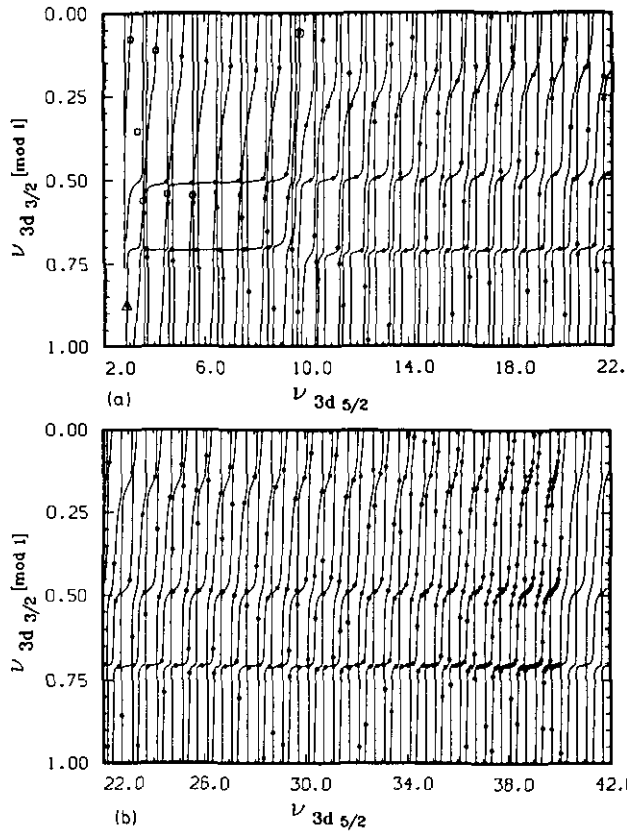

Figure 7. Lu–Fano plot of the autoionizing $J = 2^e$ levels in the $-\nu_{3d_{3/2}}$ (mod 1) against $\nu_{3d_{5/2}}$ plane. The curves and theoretical energy levels (●, ⊙, △) are calculated with the *jj*-coupled effective reaction matrix $K_{\text{eff}}^{J=2}$. (△): corresponds to the P_2' level, (○): to the 4p5p $^3D_2$ level and the squares to experimental levels (SC).

the observed $J = 2$ levels (SC) and the dots to the calculated energy positions of unobserved levels. The energy positions of the levels located below 62 500 cm^{-1} are given in the third column of table 7.

Compared to figure 3, this plot shows a more regular pattern of Rydberg series converging to the $3d_{3/2}$ threshold, periodically perturbed by levels converging to the higher $3d_{5/2}$ threshold. The $3d_{3/2}ns_{1/2}$, $3d_{3/2}nd_{3/2}$ and $3d_{3/2}nd_{5/2}$ series are characterized by quantum defects around 2.3, 0.5 and 0.8 respectively. Most of the $3d_{3/2}ns_{1/2}$ levels lie close to a horizontal line while larger deviations occur for $3d_{3/2}nd_{3/2}$ and, more significantly, $3d_{3/2}nd_{5/2}$ levels, showing that these latter series interact more strongly with series converging to higher thresholds $3d_{5/2}$ or $4p_{1/2,3/2}$. The vertical branches correspond to $3d_{5/2}nl$ perturbers except a branch near $\nu_{d_{5/2}} \simeq 9.8$ due to the 4p5p $^3D_2$ level. We have analysed in detail the wavefunctions of energy levels below 62 500 cm^{-1}. Our conclusion for the P_2' and 4p5p $^3D_2$ levels confirm the results obtained in *LS*-coupling. Low-lying 3d*nl* levels are better described in *LS*-coupling than in *jj*-coupling while the opposite holds for high-lying levels. Corresponding labels are given in table 7. Detailed analysis shows that the pattern of interacting series evolves as $\nu_{d_{5/2}}$ increases, this evolution being related to the

Table 7. Energy positions, effective quantum numbers and *jj* or *LS* designations of $J = 2^e$ autoionizing resonances below 62500 cm^{-1}. The two first columns correspond to the positions of maxima in the calculated photoionization spectra from the 4s4p $^1P_1$ and $^3P_1$ levels respectively. The energies in the third column, effective quantum numbers and labels are obtained from $K_{eff}^{J=2}$.

E (cm^{-1})					
4s4p $^1P_1$	4s4p $^3P_1$	$K_{eff}^{J=2}$	$\nu_{d_{5/2}}$	$\nu_{d_{3/2}}$	Label
49526		49698.4	2.87	2.88	$4p^2\ ^1D_2$
51381	51375	51373.8	3.07	3.08	$3d4d\ ^3D_2$
53966	53965	53963.8	3.48	3.49	$3d4d\ ^3F_2$
54376	54375	54360.9	3.56	3.57	$3d4d\ ^1D_2$
54501	54495	54498.0	3.59	3.60	$3d4d\ ^3P_2$
		54961.2	3.69	3.70	$3d_{3/2}6s$
56226	55525	55075.9	3.72	3.73	$3d_{5/2}6s$
56476	56475	56474.0	4.10	4.11	$3d5d\ ^3D_2$
57556	57555	57555.0	4.48	4.50	$3d5d\ ^3F_2$
57656	57655	57653.5	4.52	4.55	$3d5d\ ^1D_2$
57706	57705	57705.6	4.55	4.57	$3d5d\ ^3P_2$
	58220	58007.7	4.68	4.71	$3d_{3/2}7s$
		58076.1	4.71	4.74	$3d_{5/2}7s$
58791	58795	58789.7	5.10	5.13	$3d_{3/2}6d_{5/2}$
59341		59343.7	5.47	5.51	$3d_{3/2}6d_{3/2}$
59381	59385	59383.7	5.50	5.54	$3d_{5/2}6d_{3/2}$
59416	59420	59419.1	5.52	5.57	$3d_{5/2}6d_{5/2}$
	59705	59589.9	5.66	5.71	$3d_{3/2}8s$
59616		59652.3	5.71	5.76	$3d_{5/2}8s$
60051	60051	60051.4	6.08	6.15	$3d_{3/2}7d_{5/2}$
60366	60367	60366.3	6.43	6.51	$3d_{3/2}7d_{3/2}$
60391	60391	60390.8	6.46	6.54	$3d_{5/2}7d_{3/2}$
60426		60425.5	6.51	6.59	$3d_{5/2}7d_{5/2}$
60470.5		60517.8	6.63	6.71	$3d_{3/2}9s$
60546.5	60601	60578.7	6.71	6.79	$3d_{5/2}9s$
60815.5	60810	60815.6	7.06	7.16	$3d_{3/2}8d_{5/2}$
61005.5	61007	61007.0	7.39	7.50	$3d_{3/2}8d_{3/2}$
61028.5	61029	61028.6	7.43	7.55	$3d_{5/2}8d_{3/2}$
61061.5	61064	61062.9	7.49	7.61	$3d_{5/2}8d_{5/2}$
61085.5	61133	61108.2	7.58	7.71	$3d_{3/2}10s$
61137	61179	61168.7	7.71	7.84	$3d_{5/2}10s$
61312	61309	61312.4	8.02	8.17	$3d_{3/2}9d_{5/2}$
61433.5	61436	61435.9	8.33	8.50	$3d_{3/2}9d_{3/2}$
61454.5	61457	61456.9	8.39	8.56	$3d_{5/2}9d_{3/2}$
61487	61481.5	61490.9	8.48	8.65	$3d_{5/2}9d_{5/2}$
61499.5	61515	61506.5	8.52	8.70	$d_{3/2}11s$
61535.5	61568	61566.4	8.70	8.89	$3d_{5/2}11s$
61647	61644	61649.7	8.96	9.17	$3d_{3/2}10d_{5/2}$
61729	61735	61735.9	9.26	9.48	$3d_{3/2}10d_{3/2}$
61754	61753.5	61753.9	9.32	9.55	$3d_{5/2}10d_{3/2}$
61760.5	61787	61785.4	9.44	9.68	$3d_{3/2}12s$
61788.5		61791.7	9.46	9.71	$3d_{5/2}10d_{5/2}$
61814.5	61863.5	61835.6	9.64	9.90	$3d_{5/2}12s$
	61827.5	61871.6	9.79	10.06	$4p5p\ ^3D_2$
61910.5	61926.5	61929.3	10.05	10.34	$3d_{3/2}11d_{5/2}$
61958	61961	61961.0	10.19	10.50	$3d_{3/2}11d_{3/2}$
61994.5	61992	61991.3	10.34	10.66	$3d_{5/2}11d_{3/2}$

Table 7. (continued)

E (cm^{-1})					
4s4p $^1P_1$	4s4p $^3P_1$	$K_{eff}^{J=2}$	$\nu_{d_{5/2}}$	$\nu_{d_{3/2}}$	Label
61 975		62 005.3	10.42	10.74	$3d_{3/2}13s$
62 012.5	61 014.5	62 014.8	10.46	10.80	$3d_{5/2}11d_{5/2}$
62 037	62 060	62 062.4	10.72	11.08	$3d_{5/2}13s$
62 090.5	62 093	62 093.7	10.90	11.28	$3d_{3/2}12d_{5/2}$
62 123	62 126	62 125.6	11.10	11.49	$3d_{3/2}12d_{3/2}$
62 136.5		62 154.7	11.28	11.70	$3d_{3/2}14s$
62 157.5	62 158	62 161.2	11.32	11.75	$3d_{5/2}12d_{3/2}$
62 176	62 179	62 178.3	11.44	11.88	$3d_{5/2}12d_{5/2}$
62 194.5		62 216.9	11.71	12.18	$3d_{5/2}14s$
62 228.5	62 228	62 228.5	11.80	12.28	$3d_{3/2}13d_{5/2}$
62 251.5	62 253	62 253.1	11.99	12.49	$3d_{3/2}13d_{3/2}$
62 261	62 274.5	62 277.1	12.18	12.71	$3d_{3/2}15s$
62 289	62 289	62 288.7	12.28	12.82	$3d_{5/2}13d_{3/2}$
62 302.5	62 305	62 305.1	12.42	12.98	$3d_{5/2}13d_{5/2}$
62 336	62 335	62 333.7	12.67	13.28	$3d_{3/2}14d_{5/2}$
		62 338.7	12.72	13.33	$3d_{5/2}15s$
62 353.5	62 354	62 353.5	12.86	13.49	$3d_{3/2}14d_{3/2}$
62 361	62 369.5	62 372.7	13.05	13.71	$3d_{3/2}16s$
	62 391	62 392.2	13.24	13.94	$3d_{5/2}14d_{3/2}$
62 402	62 404	62 403.8	13.38	14.10	$3d_{5/2}14d_{5/2}$
62 409.5	62 421	62 420.5	13.57	14.31	$3d_{3/2}15d_{5/2}$
62 425.5		62 433.0	13.71	14.48	$3d_{5/2}16s$
62 434	62 434	62 434.2	13.72	14.50	$3d_{3/2}15d_{3/2}$
62 442.5	62 446	62 449.3	13.90	14.71	$3d_{3/2}17s$
62 473	62 473	62 473.3	14.20	15.07	$3d_{5/2}15d_{3/2}$
62 480.5	62 481	62 480.6	14.30	15.19	$3d_{3/2}16d_{5/2}$
62 482.5		62 493.3	14.48	15.38	$3d_{5/2}15d_{5/2}$
62 499		62 499.7	14.57	15.50	$3d_{3/2}16d_{3/2}$

presence of the 4p5p perturbers. So for example the quantum defect of $3d_{5/2}nd_{3/2}$ (respectively $3d_{5/2}nd_{5/2}$) series increases from 0.50 to 0.80 (respectively 0.48 to 0.70) as n increases from 6 to 15. In the same energy range the quantum defect of the $3d_{5/2}ns$ series is almost constant, being equal to 2.29 ± 0.01 for $6 < n < 16$ except for the $3d_{5/2}12s$ level ($\mu = 2.36$) located near the 4p5p $^3D_2$ perturber.

4.3. Photoionization spectra

We have investigated the photoionization from the 4s4p $^1P_1$ and 4s4p $^3P_1$ levels and calculated the partial cross sections corresponding to $J = 2^e$ final states. Starting from the initial state 4s4p $^1P_1$ the cross section curve has been extended below the 4s threshold by calculating the discrete oscillator strength density $\nu^3_{4s_{1/2}} f$(4s4p $^1P_1 \longrightarrow J = 2^e$) and expressing it in term of cross section. Results obtained in the 45 000–60 000 cm^{-1} energy range are shown in figure 8. The broad peak just above the ionization limit corresponds to the P'_2 level. This figure, in addition to figure 6, confirms that the P'_2 level strongly affects high-lying 4snd $^1D_2$ levels and the adjacent continuum. It is interesting to note that a similar effect has been observed in barium where the 5d8p $^1P_1$ located just at the 6s threshold dominates the oscillator strength distribution on both sides of the 6s threshold. The vertical bars correspond

to theoretical resonances which are only very weakly excited starting from the 4s4p $^1P_1$ level. The vertical arrows display the positions of some known resonances (SC). From figure 8 and table 3, our calculation correctly reproduces the positions of these resonances, except 3d4d $^3F_2$, but the existence of this level has been questionned by Risberg (1968). Finally let us note the P_2' level is not excited from the 4s4p $^3P_1$ level.

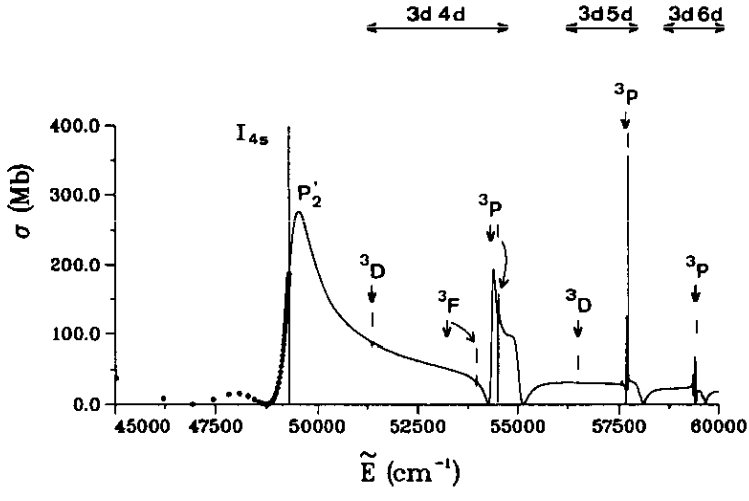

Figure 8. Calculated photoionization cross sections for the 4s4p $^1P_1 \longrightarrow J = 2^e$ process below 60000 cm^{-1}. The curve below the ionization limit is deduced from the discrete oscillator strength density $\nu^3_{4s_{1/2}} f(4s4p\ ^1P_1 \longrightarrow J = 2^e)$. The vertical bars depict some theoretical resonances. The vertical arrows indicate the positions of observed resonances (SC).

Partial photoionization cross sections for the 4s4p $^1P_1 \longrightarrow J = 2^e$ and 4s4p$^3P_1 \longrightarrow J = 2^e$ processes in the 60 000–62 500 cm^{-1} energy range are displayed in figures 9(*a*) and (*b*). The positions of maximum of the resonances are compared in table 7 to the energy positions obtained from $K_{\text{eff}}^{J=2}$. The three lists of energies are in good agreement accounting for the fact that the theoretical procedure using K_{eff} is adequate to locate the position of isolated resonances with an error comparable to their autoionization width but not suited to handle overlapping resonances. The 3d*n*s levels correspond to the broad complex features visible in figure 9 between the narrow peaks associated with the 3d*n*d levels. Since both 3d*n*s series overlap the large deviations visible in table 7 for corresponding levels are not significant. In fact, in figure 9(*a*), the structures resulting from the overlap of the $3d_{3/2}ns$ and $3d_{5/2}ns$ series exhibit some dips whose positions are very close to the energy positions obtained from $K_{\text{eff}}^{J=2}$. The differences between the widths of 3d*n*d and 3d*n*s resonances indicate that the 3d*n*d–4sϵd interaction is much smaller than the 3d*n*s–4sϵd interaction. The multiplet structure of 3d*n*d configurations can be seen in figure 9(*a*) for $n = 7$ and 8. In order of increasing energy the $3d_{3/2}nd_{5/2}$, $3d_{3/2}nd_{3/2}$, $3d_{5/2}nd_{3/2}$ and $3d_{5/2}nd_{5/2}$ levels appear successively. The former levels relatively far from the others are associated with very small peaks superposed on the $3d_{5/2}ns$ broad structures. The series $3d_{5/2}nd_{5/2}$ ($3d_{5/2}nd_{3/2}$) are depicted in figure 9(*a*) (figure 9(*b*)) by vertical bars. The heights of the 3d*n*d resonances strongly depend on the initial level. The highest peaks occurring in the photoionization spectrum from the 4s4p $^1P_1$ level correspond

for the most part to $3d_{5/2}nd_{5/2}$ levels which have the largest $^1D_2$ character. The photoionization spectrum from the 4s4p $^3P_1$ level is dominated by the $3d_{5/2}nd_{3/2}$ resonances (with maximum $^3P_2$ character) below 61 780 cm^{-1} while in the higher energy range the 4p5p $^3D_2$ perturber induces marked irregularities in the evolution of the height of the peaks. The broad complex structure depicted by B and C in figure 9(*b*) corresponds to the 4p5p $^3D_2$ level overlapping with the neighbouring $3d_{5/2}12s$ level. Finally let us note the 4p5p $^3D_2$ is not excited from the 4s4p $^1P_1$ level.

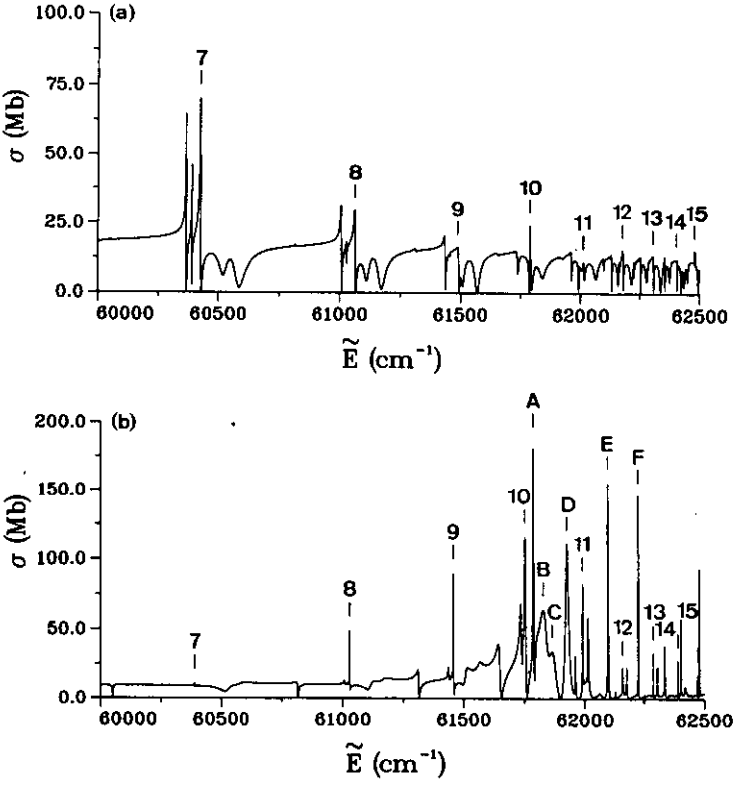

Figure 9. (*a*) Calculated photoionization cross sections for the $4s4p^1P_1 \longrightarrow J = 2^e$ process. The $3d_{5/2}nd_{5/2}$ resonances labelled by their n values are depicted by vertical bars. (*b*) Calculated photoionization cross sections for the $4s4p^3P_1 \longrightarrow J = 2^e$ process. The $3d_{5/2}nd_{3/2}$ resonances labelled by their n values as well as some other intense resonances (A: $3d_{3/2}12s + 3d_{5/2}10d_{5/2}$, C: 4p5p $^3D_2 + 3d_{5/2}12s$, D, E, F: $3d_{3/2}nd_{5/2}$ with $n = 11$, 12 and 13) are depicted by vertical bars.

5. Discussion

Several previous calculations on the bound $J = 0^e$ and $J = 2^e$ spectra of Ca have been mentioned throughout this paper and some further comparison of our results with these calculations are discussed now.

Let us first compare the MQDT parameters calculated with the R-matrix method with those obtained empirically by Armstrong *et al* (1977) and Wynne and Armstrong

(1979). The values of μ_α and of some $U_{i\alpha}$ matrix elements obtained at the 4s threshold in *LS*-coupling for the $^1S_0$, $^1D_2$ and $^3D_2$ series are compared in table 8. The empirical MQDT models fitted to energies involve simplifying assumptions concerning the number of interacting channels and the identifications of perturbers. A two-channel model was used to describe the 4s*n*s $^1S_0$ series and Wynne and Armstrong (1979) pointed out the same accuracy is achieved by assuming the perturber to be either $4p^2\ ^1S_0$ or $3d^2\ ^1S_0$. In the fitting of the $^1D_2$ series Armstrong *et al* (1977) assumed the lowest perturber to be $4p^2\ ^1D_2$ and the highest the $3d^2\ ^1D_2$ and moreover that the perturbers do not interact among themselves. In the *R*-matrix calculations no hypothesis is done on the identification of the perturbers and the d^2–p^2 interaction is accounted for.

Table 8. MQDT parameters at the 4s threshold.

i, α	1 4s*n*s	2 3d*n*d	3 4p*n*p	
		$^1S_0$		
	a	b	c	
μ_1	0.372	0.350	0.335	
μ_2	0.638		0.745	
μ_3	0.026	0.172		
U_{21}	0.327		0.18	
U_{31}	−0.175	0.23		
U_{32}	−0.250			
$i\alpha$	1 4s*n*d	2 3d*n*s	3 3d*n*d	4 4p*n*p
	$^1D_2$		$^3D_2$	
	d	e	d	f
μ_1	0.714	0.801	0.860	0.869
μ_2	0.341	0.337	0.353	0.334
μ_3	0.526	0.184	0.106	
μ_4	0.158	0.213	0.930	
U_{21}	−0.352	0.418	0.264	0.266
U_{31}	0.408	0.335	0.209	
U_{41}	−0.317	0.240	−0.160	
U_{32}	0.465	0	−0.262	
U_{42}	0.533	0	0.273	
U_{43}	−0.568	0	0.587	

[a] This work; three-channel treatment.
[b] Armstrong *et al* (1977), Wynne and Armstrong (1979); two-channel fitting with $P_0 = 4p^2\ ^1S_0$.
[c] Wynne and Armstrong (1979); two-channel fitting with $P_0 = 3d^2\ ^1S_0$.
[d] This work; four-channel calculation.
[e] Armstrong *et al* (1977); four-channel fitting.
[f] Armstrong *et al* (1977); two-channel fitting.

Table 8 shows that good agreement between calculated and fitted parameters occurs for the $^3D_2$ series only because this series is not affected by the dd–pp interaction, in contrast with the singlet series. For the $^1S_0$ and $^1D_2$ series, the μ_α values associated

with the 3d*n*d and 4p*n*p eigenchannels are completely different because of the neglect of the $3d^2$–$4p^2$ interaction in the empirical treatments. The $U_{i\alpha}$ matrix elements are also rather different, the $U_{i\alpha}$ elements set equal to zero in the empirical fits having large values in our work. This comparison between MQDT parameters either calculated with *R*-matrix method or fitted to energies under some simplifying assumptions shows the latter parameters lose part of their original physical meaning and no longer describe short-range interaction. Thus the wavefunctions calculated with fitted MQDT parameters strongly differ from those obtained with more elaborated theoretical methods. This supports the conclusion of Froese Fischer and Hansen (1981, 1985) about the inadequacy of the empirical MQDT for describing Rydberg series perturbed by an isolated perturber, such as nl^2 level.

Now we come back to table 4 which displays the pp and dd character in the four singlet levels of $3d^2$ and $4p^2$ configurations obtained using different approaches. Table 4 shows that all calculations confirm the $3d^2$ and $4p^2$ configurations interact strongly in the four levels. Thus calculations done by neglecting the strong dd–pp interaction, as for example those recently performed by Bhatia *et al* (1990), are expected to give poor results. The agreement between pp and dd characters in the P_0 and P_2 bound levels obtained using different methods is rather poor and the numbers of table 4 must deserve several comments. The W_i values (b results) obtained in the present work must be considered with care. In fact, as explained by Seaton (1983), the W_i values give a good value for the amount of channel i in a particular high-lying level. The use of the W values for low-lying levels is more doubtful. The fact that the sum of the W_{dd} coefficients obtained for the P_0 and P_0' (respectively P_2 and P_2') levels is larger than 100 indicates that W_i values for the P_0 and P_2 levels are not reliable. This probably explains the large difference between results (a) and (b) for the P_2 level. We are however more confident of the W_i values relevant to the P_0' and P_2' higher-lying levels.

The differences between results (a) and previous results (d) to (h) can be explained as follows. Firstly the MCHF results (d) and (e) as well as results (g) and (h) provided by configuration mixing calculations are obtained using finite bases which do not include the continuum in contrast with results (a). The exact wavefunctions of such strongly correlated levels are expected to critically depend on the size and composition of the basis set. This point has been verified by performing different *R*-matrix calculations with different basis sets and different sizes of the reaction volume. Percentage characters obtained in these trials differ but the dd character is always dominant in the P_0 and P_2 levels, in contradiction with results (d), (e) and (h). Calculations (d) to (h) also completely neglects core-polarization effects which are included in the *R*-matrix calculations and found to be very imporant. Finally it must be emphasized that Ca has proven particularly difficult to describe theoretically by *ab initio* method because of very sensitive centrifugal barrier effects which critically affect the 3d orbital. This point is discussed in the papers of Froese Fischer and Hansen (1981, 1985) and Vaeck *et al* (1991) dealing with bound levels of Ca but also in the paper of Greene and Kim (1987) devoted to the absorption spectra. Thus it is not very surprising that different theoretical methods give quite different percentage characters.

In close analogy with Sr (Aymar *et al* 1987, Vaeck *et al* 1988), this work emphasizes that the independent particle model fails to correctly label the $4p^2$ and $3d^2$ singlet levels of Ca. Obtaining level designations is of course of limited interest. A more important point is to test the wavefunctions by calculating observables other

than energy levels and comparing the theoretical values to experiment. The MCHF wavefunctions of Ca and Sr were recently checked by calculating lifetimes and isotope shifts (see Vaeck *et al* 1988, 1991 and references therein). Because of the known complexity of Ca, we use in this work a sophisticated model potential to describe the $e\text{–}Ca^{2+}$ interaction and an extended two-electron basis in the R-matrix calculation (200 to 400 basis functions for a given SL symmetry). When the comparison with experimental data is possible, the agreement between calculated and observed energy levels is good, giving us some confidence in the reliability of our predictions. But of course additional experimental data are highly desirable to check our calculations.

There is an obvious lack of experimental data concerning the even parity autoionizing spectrum of Ca and we hope this theoretical study will stimulate the experimentalists to investigate photoionization from low-lying $J = 1^o$ states. Starting from a $J = 1^o$ level, not only the $J = 0^e$ and $J = 2^e$ levels are excited but also the $J = 1^e$ not investigated in the present work. As done by Kompitsas *et al* (1991, 1992), the use of polarized light might help to identify the resonances. As evident from figures 4, 7 and 9 although spin–orbit effects are not negligible in the autoionizing energy range, it will be difficult to excite all the 3dnl levels starting for a given initial state and spectra corresponding to different $^1P_1^o$ and $^3P_1^o$ starting levels will be certainly required to get complete information on the 3dnl series. The 3dnl, P_0', P_2' and 4p5p $^3D_2$ levels are expected to be easier to excite from an initial state having an important dp character. For the ^3P series, the dp character is expected to be the largest for the levels labelled 3d4p ^3P in the literature. For the $^1P_1$ series, Froese Fischer and Hansen found the 3d4p $^1P_1$ perturber is spread over a large number of low-lying levels with a maximum of 10% for the lowest 4s4p $^1P_1$ level.

Note added in proof. A similar theoretical description of the 4sns $^1S_0$ and 4snd $^1D_2$ Rydberg series of calcium has been obtained by Osanai *et al* (1991) during the completion of this work.

References

Armstrong J A, Esherick P and Wynne J J 1977 *Phys. Rev.* A **15** 180
Aymar M 1987 *J. Phys. B: At. Mol. Phys.* **20** 6507
—— 1990 *J. Phys. B: At. Mol. Opt. Phys.* **23** 2697
Aymar M, Camus P and El Himdy A 1982 *J. Phys. B: At. Mol. Phys.* 15 L759
—— 1983 *Phys. Scr.* **27** 183
Aymar M, Luc-Koenig E and Watanabe S 1987 *J. Phys. B: At. Mol. Phys.* **20** 4325
Bhatia K S, Connerade J P and Makdisi Y 1990 *J. Phys. B: At. Mol. Opt. Phys.* **23** 3475
Fano U and Rau A R P 1986 *Atomic Collisions and Spectra* (New York: Academic)
Friedrich and Trefftz 1969 *J. Quant. Radiat. Transfer* **9** 333
Froese Fischer C and Hansen J E 1981 *Phys. Rev.* A **24** 631
—— 1985 *J. Phys. B: At. Mol. Phys.* **18** 4031
Giusti-Suzor A and Fano U 1984 *J. Phys. B: At. Mol. Phys.* **17** 215

Greene C H 1985 *Phys. Rev.* A **32** 1880
—— 1988 *Fundamental Processes of Atomic Dynamics* ed J Briggs, H Kleinpoppen and H Lutz (New York: Plenum)
Greene C H and Aymar M 1991 *Phys. Rev.* A **44** 1773
Greene C H and Kim L 1987 *Phys. Rev.* A **36** 2706
Kim L and Greene C H 1987 *Phys. Rev.* A **36** 4272
—— 1988 *Phys. Rev.* A **38** 2361
Kompitsas M, Cohen S, Nicolaides C A, Robaux O, Aymar M and Camus P 1990 *J. Phys. B: At. Mol. Opt. Phys.* **23** 2247
Kompitsas M, Goutis S, Aymar M and Camus P 1991 *J. Phys. B: At. Mol. Opt. Phys.* **24** 1557
—— 1992 *J. Phys. B: At. Mol. Opt. Phys.* to be submitted
Lecomte J M 1987 *J. Phys. B: At. Mol. Phys.* **20** 3645
Lee C M and Lu K T 1973 *Phys. Rev.* A **8** 1241
Lu K T 1971 *Phys. Rev.* A **4** 579
Morita N and Suzuki 1990 *Phys. Rev.* A **41** 2375
Nesbet R K and Jones H W 1977 *Phys. Rev.* A **16** 1161
Nomura T and Tatewaki H 1982 *Phys. Rev.* A **26** 1516
Osanai Y, Noro T and Sasaki F 1991 *J. Phys. B: At. Mol. Opt. Phys.* **24** 2641
Risberg G 1968 *Ark. Fys.* **37** 231
Seaton M J 1983 *Rep. Prog. Phys.* **46** 167
Sugar J and Corliss C 1985 *J. Phys. Chem. Data* **14** 51
Vaeck N, Godefroid M and Hansen J E 1988 *Phys. Rev.* A **38** 2830
—— 1991 *J. Phys. B: At. Mol. Opt. Phys.* **24** 361
Wynne J J and Armstrong J A 1979 *IBM J. Res. Dev.* **23** 490